

Calibrating Multivariate Lévy Processes with Neural Networks

Kailai Xu¹ and Eric Darve^{1,2}

¹Institute for Computational and Mathematical Engineering, Stanford University, Stanford, CA, 94305

²Mechanical Engineering, Stanford University, Stanford, CA, 94305

Abstract

Calibrating a Lévy process usually requires characterizing its jump distribution. Traditionally this problem can be solved with nonparametric estimation using the empirical characteristic functions (ECF), assuming certain regularity, and results to date are mostly in 1D. For multivariate Lévy processes and less smooth Lévy densities, the problem becomes challenging as ECFs decay slowly and have large uncertainty because of limited observations. We solve this problem by approximating the Lévy density with a parametrized functional form; the characteristic function is then estimated using numerical integration. In our benchmarks, we used deep neural networks and found that they are robust and can capture sharp transitions in the Lévy density. They perform favorably compared to piecewise linear functions and radial basis functions. The methods and techniques developed here apply to many other problems that involve nonparametric estimation of functions embedded in a system model.

1 Introduction

Lévy processes generalize the Gaussian processes by allowing the jump-diffusion. Because of their ability to allow continuous evolution and abrupt jumps of random variables [1], many models in finance, physics or biology have been built based on Lévy processes. For example, in the classical Black-Scholes model for risky assets, the price S_t of an asset at time t is governed by [2]

$$S_t = S_0 e^{\sigma B_t + \mu t} \quad (1)$$

where B_t is the standard Brownian motion, σ and μ are the standard deviation and the drift mean. To account for the excessive skewness and kurtosis in the log return distributions in empirical financial data, the model has been generalized to the exponential Lévy process

$$S_t = S_0 e^{X_t} \quad (2)$$

where X_t is a Lévy process. Yet because of the lack of analytical closed-form density functions for general Lévy processes, an exact maximum likelihood estimator is not feasible. This leads to the difficulty of calibrating Lévy processes in the presence of jumps.

The multivariate Lévy process can be described by three parameters [3]: a positive semi-definite matrix $\mathbf{A} = \Sigma \Sigma^T \in \mathbb{R}^{d \times d}$, where $\Sigma \in \mathbb{R}^{d \times d}$, a vector $\mathbf{b} \in \mathbb{R}^d$ and a measure $\nu \in \mathbb{R}^d \setminus \{0\}$. The Lévy process \mathbf{X}_t is a superposition of a Wiener process $\Sigma \mathbf{B}_t + \mathbf{b}t$, where \mathbf{B}_t is the standard i.i.d. Brownian motion, and a pure-jump Lévy process with the Lévy measure

$$\nu(A) = \frac{1}{t} \mathbb{E} \left(\sum_{s \leq t} \mathbf{1}_A(\mathbf{X}_s - \mathbf{X}_{s-}) \right) \quad (3)$$

where $\mathbf{1}_A$ is an indicator for A , i.e., $\mathbf{1}_A(\mathbf{x}) = 1$ for $\mathbf{x} \in A$ and 0 otherwise. The corresponding characteristic function is given by the Lévy-Khintchine representation [4]

$$\phi(\boldsymbol{\xi}) = \mathbb{E}[e^{i\langle \boldsymbol{\xi}, \mathbf{X}_t \rangle}] = \exp \left[t \left(i\langle \mathbf{b}, \boldsymbol{\xi} \rangle - \frac{1}{2} \langle \boldsymbol{\xi}, \mathbf{A} \boldsymbol{\xi} \rangle + \int_{\mathbb{R}^d} \left(e^{i\langle \boldsymbol{\xi}, \mathbf{x} \rangle} - 1 - i\langle \boldsymbol{\xi}, \mathbf{x} \rangle \mathbf{1}_{\|\mathbf{x}\| \leq 1} \right) \nu(d\mathbf{x}) \right) \right] \quad (4)$$

The subject of this paper is to study the nonparametric calibration of pure jump processes $\nu(\mathbf{x})$ and thus we assume $\mathbf{A} = \mathbf{0}$ and $\mathbf{b} = \mathbf{0}$ throughout the paper. In addition, we assume that ν is determined by a density function such that $\nu(ds) = \nu(\mathbf{s})d\mathbf{s}$, and we call $\nu(\mathbf{s})$ the *Lévy density*.

The traditional nonparametric estimation for Lévy processes in 1D has two regimes [5]: (1) the Lévy process X_t is observed at high frequency at times t_i , i.e., $\max_i(t_i - t_{i-1})$ is small. In this case, a large increment $X_{t_i} - X_{t_{i-1}}$ indicates that a jump occurred. For example [6] proposed nonparametric inference methods for Lévy process in this case. (2) in the low-frequency observation regime, there are zero or several jumps present within the increment $X_{t_i} - X_{t_{i-1}}$. In this case, [5] applied a deconvolution algorithm to estimate $\nu(x)$ from the empirical characteristic function. [7] discretized the Lévy density $\nu(x)$ on a grid and applied relative entropy minimization to find the optimal $\nu(x)$. We consider the latter regime and assume that the data are given at equispaced time intervals, i.e., $t_1 = \Delta t$, $t_2 = 2\Delta t$, $t_3 = 3\Delta t$, \dots

However, much of the attention in the literature has been restricted to 1D case and well-behaved $\nu(x)$. In the case where $\nu(x)$ is discontinuous, the decay of the characteristic function is very slow so accurate deconvolution in [5] requires large computational domains. Besides, [7] assigned one degree of freedom (DOF) to the discretized Lévy density $\nu(x)$ per grid point, which partially contributed to the ill-posedness of the nonlinear optimization problem. The ill-posedness problem becomes more severe in higher dimensions since DOFs grow exponentially.

In this paper, we tackle those challenges by proposing a novel approach for 2D nonparametric estimation of the Lévy density $\nu(x)$. This approach proceeds in four stages:

1. The Lévy density is approximated by a parametric functional form—such as piecewise linear functions—with parameters θ ,

$$\nu(\mathbf{x}) \approx \nu_\theta(\mathbf{x}) \quad (5)$$

2. The characteristic function is approximated by numerical integration

$$\phi(\boldsymbol{\xi}) \approx \phi_\theta(\boldsymbol{\xi}) := \exp \left[\Delta t \sum_{i=1}^{n_q} \left(e^{i\langle \boldsymbol{\xi}, \mathbf{x}_i \rangle} - 1 - i\langle \boldsymbol{\xi}, \mathbf{x}_i \rangle \mathbf{1}_{\|\mathbf{x}_i\| \leq 1} \right) \nu_\theta(\mathbf{x}_i) w_i \right] \quad (6)$$

where $\{\mathbf{x}_i, w_i\}_{i=1}^{n_q}$ are quadrature nodes and weights.

3. The empirical characteristic functions are computed given observations $\{\mathbf{X}_{i\Delta t}\}_{i=0}^n$

$$\hat{\phi}_n(\boldsymbol{\xi}) := \frac{1}{n} \sum_{i=1}^n \exp(i\langle \boldsymbol{\xi}, \mathbf{X}_{i\Delta t} - \mathbf{X}_{(i-1)\Delta t} \rangle), \quad \boldsymbol{\xi} \in \mathbb{R}^d \quad (7)$$

4. Solve the following optimization problem with a gradient based method. Here $\{\boldsymbol{\xi}_i\}_{i=1}^m$ are collocation points depending on the data.

$$\min_{\theta} \frac{1}{m} \sum_{i=1}^m \|\hat{\phi}_n(\boldsymbol{\xi}_i) - \phi_\theta(\boldsymbol{\xi}_i)\|^2 \quad (8)$$

One challenge for this approach is the error $\|\hat{\phi}_n(\boldsymbol{\xi}) - \phi(\boldsymbol{\xi})\|$ in computing the empirical characteristic function. In theory, the empirical characteristic function converges to the exact one given infinite observations. However, in practice the observations are limited and thus the empirical characteristic function is not exact. Another challenge is the discontinuity of Lévy densities. This occurs when the jump distribution experiences sudden changes in some domains.

The choice of approximation functional form $\nu_\theta(\mathbf{x})$ is essential. From the previous discussion, a potential form must have the following properties: (1) universal approximation, i.e., the capability of approximating any continuous functions given sufficient computing budget; (2) robustness to noise; (3) ability to handle discontinuity. In this paper, we apply and benchmark three popular parametric functional forms: neural networks (NN), piecewise linear functions (PL) and radial basis functions (RBF).

The neural network enjoys many favorable properties and we demonstrate empirically that it outperforms the others in several situations. On the one hand, PL consists of local basis functions and therefore DOFs with no data points nearby

around are not optimized. On the other hand, although the basis functions in RBF are global such that it suffers less from the problem PL struggles with, it is well known that RBF is susceptible to noise and discontinuity. Besides, the choice of centers and shape parameters can be tricky. However, the problems are alleviated for NN, partially because it is adaptive to non-uniform data [8], robust to noise and can overcome Gibbs phenomenon [9]. This is also demonstrated in Figure 1, where the basis functions are trained on 20 data points in a step function. NN honors the sharp transitions and does not oscillate as severely as others.

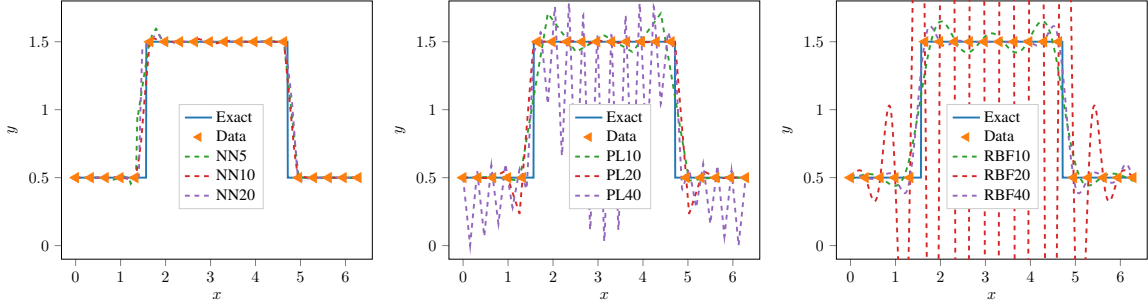


Fig. 1. Training with 20 sample points from a step function. NN x stands for neural network model with x layers, 20 neurons per hidden layer and ReLU as activation function. PL x stands for piecewise linear function with x equispaced distributed nodes. RBF x stands for radial basis functions with x equispaced distributed centers.

With the re-parametrization technique, we show that the method can also be applied to multivariate symmetric α -stable processes [10], a subclass of Lévy processes. In this case, $\nu(\mathbf{x})$ is singular at $\mathbf{x} = \mathbf{0}$, but we can re-parametrize the characteristic function as

$$\phi(\boldsymbol{\xi}) = \mathbb{E}(\exp(it\langle\boldsymbol{\theta}, \boldsymbol{\xi}\rangle)) = \exp\left[t\left(-\frac{1}{2}\langle\boldsymbol{\xi}, \mathbf{A}\boldsymbol{\xi}\rangle + i\langle\boldsymbol{\xi}, \mathbf{b}\rangle - \int_{\mathbb{S}^d} |\langle\boldsymbol{\theta}, \boldsymbol{\xi}\rangle|^\alpha \Gamma(s) ds\right)\right] \quad (9)$$

where $\Gamma(s)$ is a function defined on \mathbb{S}^d . Here we can substitute $\Gamma(s)$ by a parametrized functional form $\Gamma_\theta(s)$, apply the quadrature rule on the unit circle and minimize the discrepancy between $\hat{\phi}_n(\boldsymbol{\xi})$ and $\phi_\theta(\boldsymbol{\xi})$.

Finally, we built a toolset `LevyNN` for calibrating Lévy processes based on the open source library `ADCME.jl`. The latter is an automatic differentiation library with `TensorFlow` and `PyTorch` backends and is specially designed for scientific computing. The library automates the gradient computation and integrates the optimization workflow.

2 Nonparametric Estimation of the Lévy processes

2.1 Characteristic Function Matching Method

The characteristic function matching method [11] minimizes the discrepancy between the empirical characteristic function $\hat{\phi}_n(\boldsymbol{\xi})$ (Equation (7)) and the characteristic function $\phi(\boldsymbol{\xi})$ (Equation (4)). The rationales are: (1) As $n \rightarrow \infty$, $\hat{\phi}_n(\boldsymbol{\xi}) \rightarrow \phi(\boldsymbol{\xi})$ because of the large number law; (2) there is a one-to-one correspondence between the characteristic function $\phi(\mathbf{x})$ and the density function for $\mathbf{X}_{i\Delta t} - \mathbf{X}_{(i-1)\Delta t}$, a.k.a., $\nu(\mathbf{x})$. Consequently, we can estimate $\nu(\mathbf{x})$ from $\hat{\phi}_n(\boldsymbol{\xi})$.

2.2 Approximation to the Lévy Density

The Lévy density $\nu(\mathbf{x})$ is a mapping from the coordinates $\mathbf{x} \in \mathbb{R}^2$ to \mathbb{R} . We first truncate the infinite computational domain to $\mathbf{x} \in [-M, M]^2$ and then approximate $\nu(\mathbf{x})$ with $\nu_\theta(\mathbf{x})$. In the following we discuss three functional forms for $\nu_\theta(\mathbf{x})$ (Figure 2).

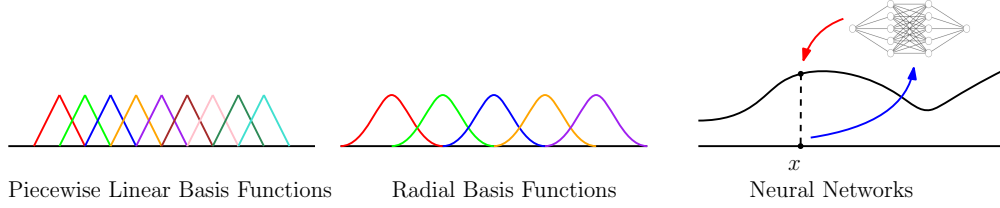


Fig. 2. Different functional forms in 1D. In PL and RBF, the target function are approximated by linear combination of basis functions; in NN, it is approximated by composing linear transformations and nonlinear activation functions.

One type of neural networks (NN) is a composition of linear operations followed by a nonlinear activation function. In this paper, we consider ReLU dense neural networks, where

$$\nu_{\theta}(\mathbf{x}) = \mathbf{W}_L \text{ReLU}(\mathbf{W}_{L-1} \text{ReLU}(\cdots \text{ReLU}(\mathbf{W}_1 \mathbf{x} + \mathbf{b}_1) \cdots) + \mathbf{b}_{L-1}) + \mathbf{b}_L \quad (10)$$

here $\text{ReLU}(x) = \max(x, 0)$ and it is applied elementwise, L is the number of layers and $\theta = \{(\mathbf{W}_i, \mathbf{b}_i)\}_{i=1}^L$ are the weights and biases. For all the hidden layers, we use 20 neurons. NN is special because information at each data point is not represented by linear combination of predetermined basis functions but composing linear and nonlinear mappings.

For piecewise linear functions (PL), the computational domain is first triangulated and each vertex is associated with one DOF. The value $\nu_{\theta}(\mathbf{x})$ is linearly interpolated from the nodal values of the triangle where \mathbf{x} is located. θ consists of all those DOFs. In this paper, we obtain the triangulation by splitting each square cell into two triangles on a uniform grid. One disadvantage of PL is the local DOF problem, where the DOFs with no data points nearby are not trained.

For radial basis functions (RBF), we have

$$\nu_{\theta}(\mathbf{x}) = \sum_{i=1}^M a_i \frac{1}{\sqrt{(\mathbf{x} - \mathbf{x}_i)^2 + c^2}} \quad (11)$$

where $\{a_i\}_{i=1}^M$ are coefficients, $\{\mathbf{x}_i\}_{i=1}^M$ are centers, c is the shape parameter. In this paper, the centers are chosen as the grid points on a uniform grids. c is given by the grid step size, suggested by [12]. Although the basis functions are global, the coefficients in RBF are more affected by data points that are closer to the corresponding centers. Hence, we expect RBF also suffers from the local DOF problem like PL.

2.3 Numerical Approximation to the Characteristic Function

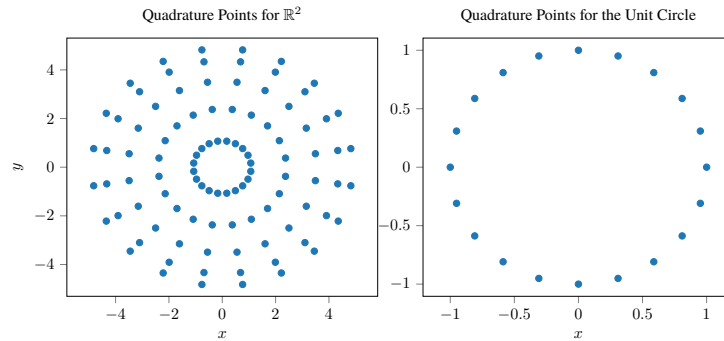


Fig. 3. Quadrature points used for \mathbb{R}^2 and the unit circle. To avoid bloated plots, we show fewer quadrature points with order $n_q = 100$, $n_q = 20$ respectively.

We assume that $\nu(\mathbf{x})$ decays as $\|\mathbf{x}\| \rightarrow \infty$, we use the quadrature rule on the truncated domain $\{(x, y) : x^2 + y^2 < M^2\}$ for approximating the integral in Equation (4)

$$\int_{\mathbb{R}^2} \left(e^{i\langle \boldsymbol{\xi}, \mathbf{x} \rangle} - 1 - i\langle \boldsymbol{\xi}, \mathbf{x} \rangle \mathbf{1}_{\|\mathbf{x}\| \leq 1} \right) \nu(\mathbf{x}) d\mathbf{x} \approx \sum_{i=1}^{n_q} \left(e^{i\langle \boldsymbol{\xi}, \mathbf{x}_i \rangle} - 1 - i\langle \boldsymbol{\xi}, \mathbf{x}_i \rangle \mathbf{1}_{\|\mathbf{x}_i\| \leq 1} \right) \nu_{\boldsymbol{\theta}}(\mathbf{x}_i) w_i$$

The quadrature points and weights $\{(\mathbf{x}_i, w_i)\}_{i=1}^{n_q}$ are obtained according to [13]. For multivariate stable processes in the following, we use quadrature rules on the unit circle. Figure 3 shows examples of quadrature points with order $n_q = 100$ and $n_q = 20$.

Consequently, we obtain the expression for the approximation to the characteristic function

$$\phi(\boldsymbol{\xi}) \approx \phi_{\boldsymbol{\theta}}(\boldsymbol{\xi}) := \exp \left[\Delta t \sum_{i=1}^n \left(e^{i\langle \boldsymbol{\xi}, \mathbf{x}_i \rangle} - 1 - i\langle \boldsymbol{\xi}, \mathbf{x}_i \rangle \mathbf{1}_{\|\mathbf{x}_i\| \leq 1} \right) \nu_{\boldsymbol{\theta}}(\mathbf{x}_i) w_i \right] \quad (12)$$

2.4 Optimization

The characteristic function matching method requires minimizing the discrepancy between $\hat{\phi}_n(\boldsymbol{\xi})$ and $\phi_{\boldsymbol{\theta}}(\boldsymbol{\xi})$. For computation, we consider a set of collocation points $\{\boldsymbol{\xi}_i\}_{i=1}^m$ uniformly drawn from $[-M', M']^2$ and solve the nonlinear least square problem

$$\min_{\boldsymbol{\theta}} L(\boldsymbol{\theta}) := \frac{1}{m} \sum_{i=1}^m \|\hat{\phi}_n(\boldsymbol{\xi}_i) - \phi_{\boldsymbol{\theta}}(\boldsymbol{\xi}_i)\|^2 \quad (13)$$

The choice of M' is based on data. For example, we can choose M' such that $|\hat{\phi}_n(\boldsymbol{\xi})|$ is smaller than a certain value for $\boldsymbol{\xi} \in \mathbb{R}^2 \setminus [-M', M']^2$.

The optimization problem Equation (13) is solved with `ADCFME`. It computes the gradient $\nabla L(\boldsymbol{\theta})$ using automatic differentiation [14] and applies a gradient-based optimizer such as `L-BFGS-B` [15] for minimization. The considerable flexibility makes it easy to test different approximation functional forms $\nu_{\boldsymbol{\theta}}(\mathbf{x})$ without deriving and implementing new gradients or optimization procedures.

2.5 Multivariate α -Stable Process: Re-parametrization

For the multivariate symmetric α -stable distribution, the characteristic function of the increment $X_{i\Delta t} - X_{(i-1)\Delta t}$ is given by the following theorem [16]

Theorem 1 \mathbf{X} is a symmetric α -stable vector in \mathbb{R}^d with $0 < \alpha < 2$ if and only if there exists a unique symmetric finite measure Γ on the unit sphere \mathbb{S}^d such that

$$\phi(\boldsymbol{\xi}) = \mathbb{E}(\exp(i\Delta t \langle \mathbf{X}, \boldsymbol{\xi} \rangle)) = \exp \left(-\Delta t \int_{\mathbb{S}^d} |\langle \mathbf{s}, \boldsymbol{\xi} \rangle|^\alpha \Gamma(ds) \right) \quad (14)$$

Γ is the spectral measure of the symmetric α -stable vector \mathbf{X} .

We assume that Γ is determined by a density function such that $\Gamma(ds) = \Gamma(\mathbf{s})d\mathbf{s}$. The previous procedure will fail because $\nu(\mathbf{x})$ is singular at $\mathbf{x} = \mathbf{0}$ thus the given quadrature rule is unable to handle. For example, when $\Gamma(\mathbf{s}) = 1$, the corresponding Lévy density satisfies [17]

$$\nu(\mathbf{x}) \propto \frac{1}{\|\mathbf{x}\|^{\alpha+2}}, \quad \|\mathbf{x}\| \rightarrow 0 \quad (15)$$

Instead of working with $\nu(\mathbf{x})$, we approximate Equation (14) directly. For calibrating the multivariate symmetric α -stable process, we apply the quadrature rule $\{(\mathbf{s}_i, w_i)\}_{i=1}^{n_q}$ on a unit circle instead of \mathbb{R}^2 and we obtain

$$\phi(\boldsymbol{\xi}) \approx \phi_{\boldsymbol{\theta}}(\boldsymbol{\xi}) := \exp(i\Delta t \langle \boldsymbol{\theta}, \boldsymbol{\xi} \rangle) = \exp \left(-\Delta t \sum_{i=1}^{n_q} |\langle \boldsymbol{\xi}, \mathbf{s}_i \rangle|^\alpha \Gamma_{\boldsymbol{\theta}}(\mathbf{s}_i) w_i \right) \quad (16)$$

Function	NN5	NN10	NN20	PL10	PL20	PL40	RBF10	RBF20	RBF40
Step	0.7500	0.7499	0.7498	0.7493	0.7494	0.7500	0.7482	0.7483	0.7504
Constant	0.7499	0.7500	0.7500	0.7500	0.7500	0.7499	0.7500	0.7500	0.7499

Table 1. Estimated α for different methods and test functions. The exact fractional index α is 0.75. We can see that the current method is able to learn α quite accurately, regardless of the choices of basis functions.

We have the additional constraint $\Gamma(\mathbf{s}) = \Gamma(-\mathbf{s})$ according to Theorem 1. This is enforced directly by the functional form Γ_θ . For example, we assume $\Gamma_\theta(\mathbf{s}) = \Gamma'_\theta(\mathbf{s}) + \Gamma'_\theta(-\mathbf{s})$, where $\Gamma'_\theta(\mathbf{s})$ is NN, PL or RBF in the 1D domain $[0, 2\pi)$ (since there exists a one-to-one correspondence between \mathbb{S}^2 and $[0, 2\pi)$).

3 Numerical Results

We now present the results of numerical experiments. We first compare the accuracy of three functional forms based on exact characteristic function, ignoring the uncertainty from observations. Then we apply and compare the functional forms to symmetric α -stable processes and general Lévy processes in the presence of uncertainty from observations. We show that NN has very favorable properties in terms of being robust and capturing sharp transitions.

3.1 Multivariate α -Stable Processes: Estimation from Exact Empirical Characteristic Functions

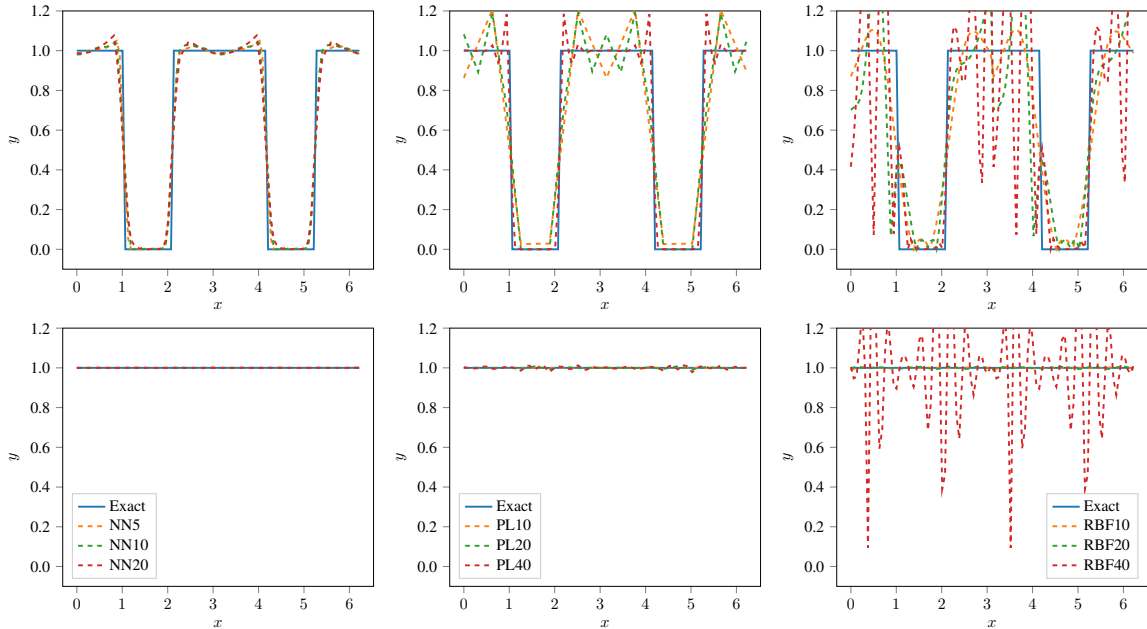


Fig. 4. Estimated $\Gamma_\theta(\mathbf{s})$ from exact characteristic functions with different methods. The $x \in [0, 2\pi)$ axis corresponds to the angle of \mathbf{s} . For details about legend abbreviations, see Figure 4.

In this example, we assume that $\phi(\boldsymbol{\xi})$ is computed with accurate numerical quadrature rules $n_q = 10000$ for

$$\Gamma(\mathbf{s}) = \mathbf{1}_{|s_1| > 0.5}(\mathbf{s}), \text{ and } \Gamma(\mathbf{s}) = 1, \mathbf{s} = (s_1, s_2), \mathbf{s} \in \mathbb{S}^2 \quad (17)$$

hence the error is negligible for estimating $\phi(\boldsymbol{\xi})$. We assume $\Delta t = 0.5$, $\alpha = 0.75$, and $n_q = 100$ for approximating $\phi_\theta(\boldsymbol{\xi})$. The results in Figure 4 indicate that NN can capture the sharp transition better than others. For PL, if DOFs

Function	NN5	NN10	NN20	PL10	PL20	PL40	RBF10	RBF20	RBF40
Step	1.5164	1.5156	1.5162	1.5151	1.5166	1.5169	3.2155	1.5154	1.5171
Constant	1.5331	1.5329	1.5329	1.5330	1.5329	1.5330	1.5329	1.5329	1.5330

Table 2. Estimated α for different methods and test functions. The reference fractional index α is 1.5. For step functions, if we use too few centers for radial basis functions, the estimation is not accurate (RBF10). This is also demonstrated in Figure 5.

are too few, it is unable to capture the transition; however, too many DOFs results in that some of them are not trained. For RBF, results for RBF40 implies that too few data points compared to the number of centers make the optimization problem ill-posed. Besides, RBF fails to capture the sharp transitions.

The fractional indices are estimated quite accurately (Table 1). This implies that compared to the “directional” information of the jump, the heavy tail information is easier to capture.

3.2 Multivariate α -Stable Processes: Estimation from Observations

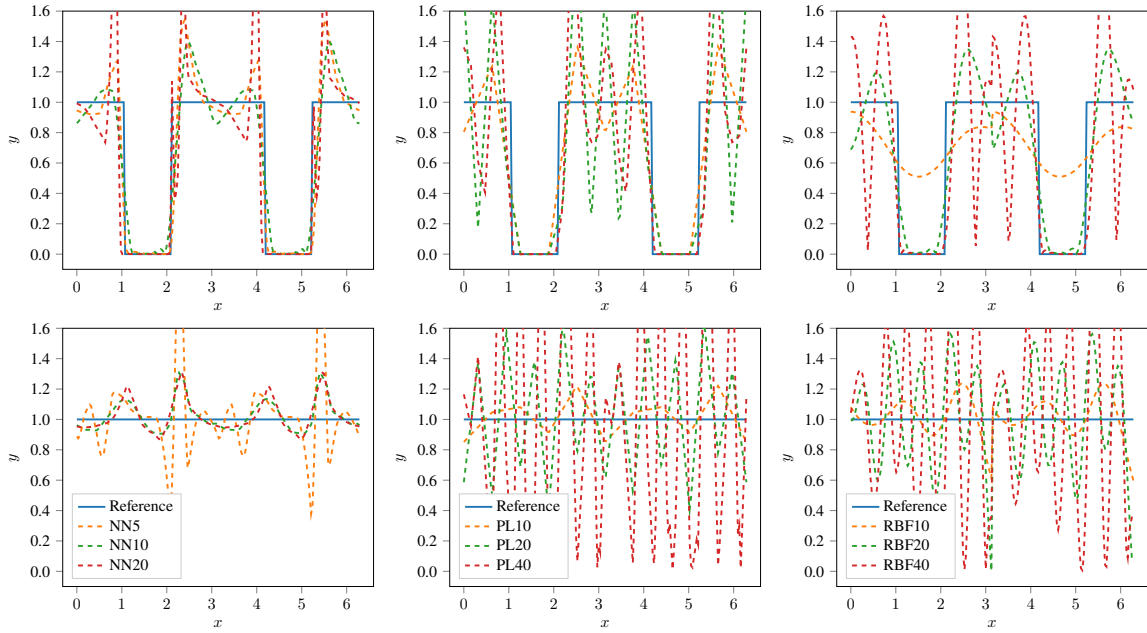


Fig. 5. Estimated $\Gamma_\theta(\mathbf{s})$ from observations with different methods. The $x \in [0, 2\pi)$ axis corresponds to the angle of \mathbf{s} . For details about legend abbreviations, see Figure 4.

Now we consider estimating the multivariate α -stable process from $m = 1000$ observations. Different from last section, $\phi(\boldsymbol{\xi})$ is unknown and is estimated with $\hat{\phi}_n(\boldsymbol{\xi})$. The difference $|\hat{\phi}_n(\boldsymbol{\xi}) - \phi(\boldsymbol{\xi})|$ introduces additional uncertainty, which can also be interpreted as “noise” in the nonlinear optimization problem.

The results in Figure 5 implies that NN is most robust in either case. The α indices are properly estimated as expected in Table 2, except for the step function and RBF10 case because of the noise.

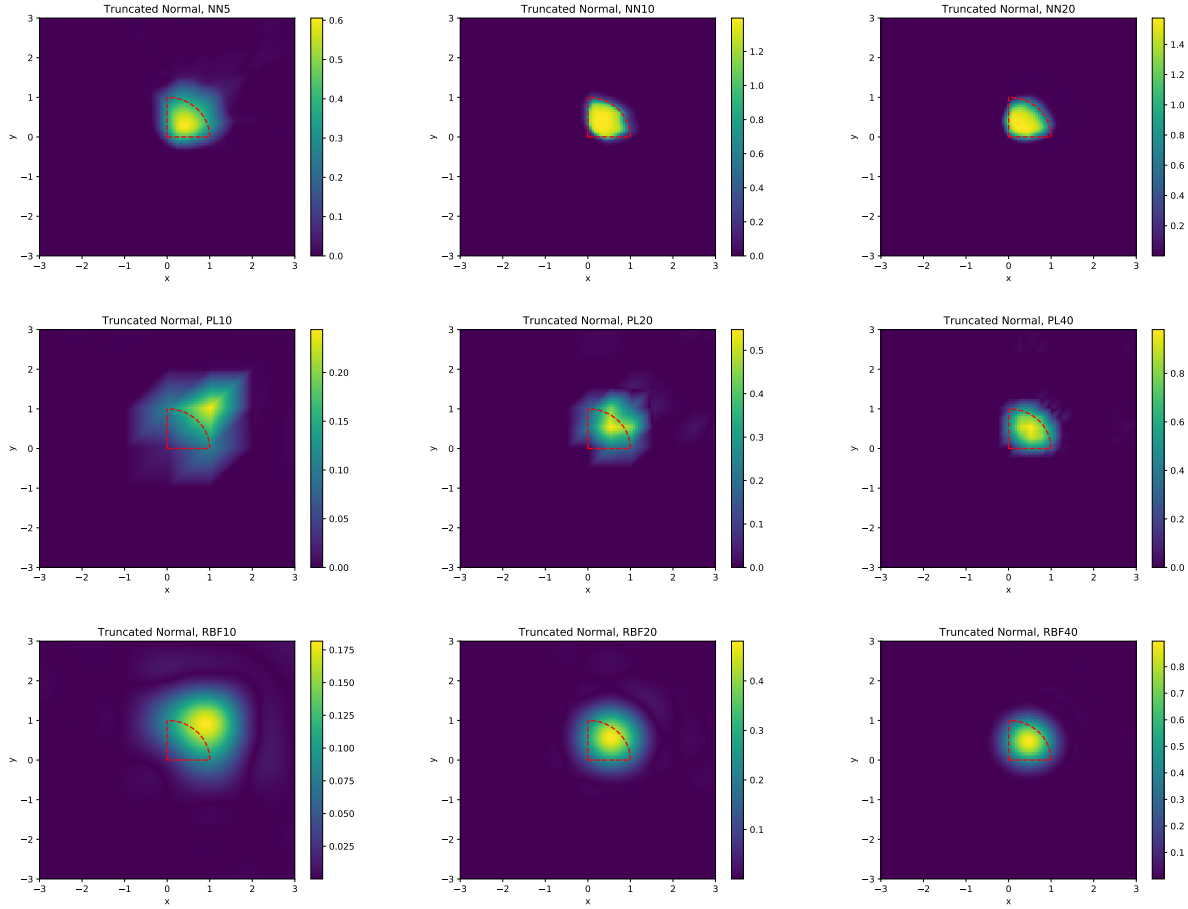


Fig. 6. Estimated $\nu_\theta(\mathbf{x})$ from observations with different methods. The intercepted arc of the dashed red sector is $\{(x, y) : x^2 + y^2 = 1, x \geq 0, y \geq 0\}$. The sector indicates the area with most of the density for the reference $\nu(\mathbf{x})$. For details about subtitle abbreviations, see Figure 4.

3.3 Multivariate Lévy Processes.

In this example, we consider the Lévy process where the jump distributions are truncated normal distributions. The Lévy density has the expression

$$\nu(\mathbf{x}) = \frac{2}{\pi} \exp\left(-\frac{\|\mathbf{x}\|^2}{2}\right) \mathbf{1}_{\mathbf{x} \in \mathbb{R}_+^2} \quad (18)$$

The density $\nu(\mathbf{x})$ is only nonzero for $\mathbf{x} \in \mathbb{R}_+^2$ and has sharp transition at axes $x = 0$ and $y = 0$ in the first quadrant. In our experiment, we assume $\Delta t = 0.5$, $m = 10000$, $n_q = 4096$. The data $\{\mathbf{X}_{i\Delta t}\}_{i=1}^n$ are simulated according to [17]. Notably, NN captures the sharp transition (Figure 6). The results from PL shows artifacts because of the localized DOFs. Despite properly indicating the location of the major density mass, RBF creates a smooth profile of the density distribution.

3.4 Application to Stock Markets.

Finally, we apply the developed procedure to a stock market example. We investigate 12 stocks from 01/01/2016 to 08/01/2019, which are from the technology sector (MSFT, AAPL, AMZN, GOOG), the financial sector (JPM, C, WFC, CME) and the energy sector (EOG, XOM, COG, MPC). The α index is computed for each pair of stocks. The stock prices are turned into the log return and then shifted such that data for each stock are unbiased.

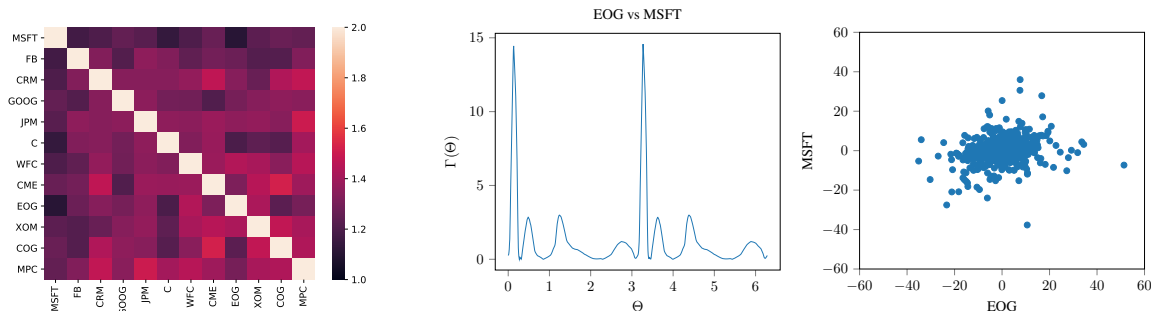


Fig. 7. The first plot shows the pairwise α indices. For each stock, the α index against itself is not computed. The right two plots show the calibrated $\Gamma_{\theta}(s)$ and shifted log return for EOG and MSFT. Here $s = (\cos(\Theta), \sin(\Theta))$

We model the pairwise shifted log return of the stocks by a 2D symmetric α -stable process with unknown α and $\Gamma(s)$. Figure 7 shows the estimated pairwise α indices. Most of the indices are between 1.1 and 1.5. This implies that there does exist jumps in the pairwise log return changes. We also show $\Gamma(s)$ for EOG vs. MSFT. We identify 4 peaks in the plot, which indicate that there is a larger tendency for price to jump in those 4 directions compared to nearby directions.

4 Conclusion

We have proposed a novel nonparametric estimation approach for Lévy processes and compared three approximation functional forms: (1) neural network; (2) piecewise linear functions; (3) radial basis functions. We found that for the tested cases the neural network performed best for being robust to noise and capturing sharp transitions. However, one should not expect that neural networks are always superior to others. Most likely, a certain functional form may be more suitable to a class of problems, since the performance highly depends on the characteristics of the training data.

Besides Lévy processes, the same idea—approximating an unknown function in a system model with the neural network, and training by matching the model outputs with observations—can be applied to many other fields as well. For example, in mechanical engineering, constitutive laws have been reconstructed from observed displacement data [8]; in general, coupled partial differential equation systems, closure relations are discovered from observations [9]. In the future, a deeper understanding of the neural network approximation properties and improvement of the training algorithm will broaden the applications of the nonparametric estimation approach.

References

- [1] Song X Chen, Aurore Delaigle, and Peter Hall. Nonparametric Estimation for a Class of Lévy Processes. *Journal of Econometrics*, 157(2):257–271, 2010.
- [2] Enrique Figueroa-Lopez and Christian Houdré. Nonparametric Estimation for Lévy Processes with a view Towards Mathematical Finance. *arXiv preprint math/0412351*, 2004.
- [3] Christian Menn and Svetlozar T Rachev. Calibrated FFT-based Density Approximations for α -stable Distributions. *Computational statistics & data analysis*, 50(8):1891–1904, 2006.
- [4] Antonis Papapantoleon. An Introduction to Lévy Processes with Applications in Finance. *arXiv preprint arXiv:0804.0482*, 2008.
- [5] Michael H Neumann, Markus Reiß, et al. Nonparametric Estimation for Lévy Processes from Low-frequency Observations. *Bernoulli*, 15(1):223–248, 2009.

- [6] Fabienne Comte and Valentine Genon-Catalot. Nonparametric Estimation for Pure Jump Lévy Processes Based on High Frequency Data. *Stochastic Processes and their Applications*, 119(12):4088–4123, 2009.
- [7] Rama Cont and Peter Tankov. Nonparametric calibration of jump-diffusion option pricing models. *Journal of computational finance*, 7:1–49, 2004.
- [8] Daniel Z Huang, Kailai Xu, Charbel Farhat, and Eric Darve. Predictive Modeling with Learned Constitutive Laws from Indirect Observations. *arXiv preprint arXiv:1905.12530*, 2019.
- [9] Kailai Xu and Eric Darve. The Neural Network Approach to Inverse Problems in Differential Equations. *arXiv preprint arXiv:1901.07758*, 2019.
- [10] Mamikon Gulian, Maziar Raissi, Paris Perdikaris, and George Karniadakis. Machine Learning of Space-fractional Differential Equations. *arXiv preprint arXiv:1808.00931*, 2018.
- [11] Jun Yu. Empirical Characteristic Function Estimation and its Applications. *Econometric reviews*, 23(2):93–123, 2004.
- [12] Yue Wu, Hui Wang, Biaobiao Zhang, and K-L Du. Using Radial Basis Function Networks for Function Approximation and Classification. *ISRN Applied Mathematics*, 2012, 2012.
- [13] Ronald Cools and Kyung Joong Kim. A Survey of Known and New Cubature Formulas for the Unit Disk. *Korean Journal of Computational & Applied Mathematics*, 7(3):477–485, 2000.
- [14] Atilim Gunes Baydin, Barak A Pearlmutter, Alexey Andreyevich Radul, and Jeffrey Mark Siskind. Automatic Differentiation in Machine Learning: a Survey. *Journal of Machine Learning Research*, 18:1–43, 2018.
- [15] Yu-Hong Dai. A Perfect Example For the BFGS Method. *Mathematical Programming*, 138(1-2):501–530, 2013.
- [16] Gennady Samorodnitsky, Murad S Taqqu, et al. Lévy Measures of Infinitely Divisible Random Vectors and Slepian Inequalities. *The Annals of Probability*, 22(4):1930–1956, 1994.
- [17] John P Nolan. An Overview of Multivariate Stable Distributions. Online: <http://academic2.american.edu/~jpnolan/stable/overview.pdf>, 2008.